FULL PAPER   **Open Access**

Along-strike variations in temperature and tectonic tremor activity along the Hikurangi subduction zone, New Zealand

Suguru Yabe[1*], Satoshi Ide[1] and Shoichi Yoshioka[2]

Abstract

In the Hikurangi subduction zone, situated along the east coast of the North Island, New Zealand, where the old oceanic Pacific Plate is subducting beneath the Australian Plate, several slow slip events and tectonic tremors have recently been documented. These observations are somewhat surprising because such slow seismic phenomena tend to be common in subduction zones where relatively young oceanic plate is subducting. The locations of tectonic tremors, down-dip limit of slow slip events and seismic coupling transition change along strike from greater depths in the south to shallower depths in the north, suggesting significant along-strike variations in the characteristics of the plate interface. Similar along-strike variations have been observed for other characteristic features of the Hikurangi subduction zone. Here, we demonstrate that along-strike variations observed for tectonic tremors, slow slip events, and seismic coupling can be explained by lateral differences in the thermal structure of the subduction zone, which are controlled mainly by variations in convergence rate and friction along the plate interface. To demonstrate this, we first confirm that tectonic tremors occur around the plate interface. Then, we calculate the thermal structure of the Hikurangi subduction zone using a two-dimensional finite difference code. To explain the along-strike variation in the heat flow observed in the forearc region, temperatures along the plate interface should be systematically higher in the northern region than in the southern region, which we interpret as a consequence of higher convergence rates and greater frictional heating in the northern region. We compare the along-strike variation of seismic characteristics with calculated thermal structure and highlight that this along-strike variation in temperature controls the depth of the brittle-ductile transition, which is consistent with the observed spatial variations in tectonic tremors, down-dip limit of slow slip events and seismic coupling. Our results suggest that tectonic tremors recorded within subduction zones reflect the transient rheology of the materials being subducted, which is controlled by variations in temperature along the plate interface.

Keywords: New Zealand; Subduction zone; Tectonic tremor; Slow earthquake; Thermal structure

Background

Tectonic tremors, or non-volcanic tremors (Obara 2002), have been discovered in many subduction zones worldwide, and they represent successive small slip events along the plate interface (Ide et al. 2007; Shelly et al. 2007a), often associated with slow slip events (SSEs, e.g., Rogers and Dragert 2003). They tend to occur where a young oceanic plate (<50 Ma) is subducting, such as in the Nankai, Alaska, Cascadia, Mexico, Costa Rica, and south Chile subduction zones (e.g., Obara 2002; Rogers and Dragert 2003; Payero et al. 2008; Brown et al. 2009; Peterson and Christensen 2009; Brudzinski et al. 2010; Ide, 2012). On the other hand, tectonic tremors have never been recorded where the old plate is subducting, except for the Hikurangi subduction zone located along the east coast of the North Island of New Zealand (Fry et al. 2011; Kim et al. 2011; Ide 2012). Therefore, the occurrence of tremors appears to be primarily controlled by the age and thermal structure of the subduction zone.

Tectonic tremors are located at the bottom edge of a seismic coupling region in subduction zones, as inferred from geodetic observations (Gomberg and the Cascadia

* Correspondence: yabe@eps.s.u-tokyo.ac.jp
[1]Department of Earth and Planetary Science, The University of Tokyo, 7-3-1, Hongo, Bunkyo, Tokyo 113-0033, Japan
Full list of author information is available at the end of the article

2007 and Beyond Working Group 2010; Liu et al. 2010). Therefore, temperatures around a tremor source region are expected to be higher than in the source region of ordinary interplate earthquakes. The higher temperatures could be responsible for tectonic tremors having characteristics that differ from those of ordinary earthquakes, especially the high sensitivity to small stress change exerted by tide and surface waves (e.g., Rubinstein et al. 2007; Shelly et al. 2007b). This high sensitivity may reflect a critical stress state, which results from the existence of a high-pressure pore fluid, dehydrated from the subducted slab, around the tremor source region. Mineralogical studies show that a young and warm oceanic plate would be dehydrated at relatively shallow depths, whereas an old and cold plate remains hydrated at the comparatively deep levels where tectonic tremors are thought to originate (Peacock 2009). However, some studies have argued against a causal relationship between temperature and tectonic tremor activity and have invoked other mechanisms to explain tectonic tremors (Brown et al. 2009; Peacock 2009).

As such, the possible influence of temperature on the tectonic tremor activity is currently an important problem under discussion in the field of seismology. Therefore, in this multidisciplinary study, we address this problem by carrying out a regional-scale seismic/thermal study of the Hikurangi subduction zone, off the North Island, New Zealand. It is a unique place in the sense that we have observed fairly large along-strike variations in both the slow earthquake activity and the observed heat flow within the subduction zone, which provide us a good opportunity to investigate the relation between them.

The remainder of this manuscript is organized as follows. An overview of tremor activity and tectonic setting is provided in the next section. In the 'Investigation of tectonic tremor events' section, we detect and locate tectonic tremors in the central part of Northern Island where tectonic tremors were already detected by some previous seismic studies. Then, we constrain the source depths of these tectonic tremors relative to the location of the plate interface, which was poorly constrained in the previous studies. The thermal structure of the Hikurangi subduction zone is modeled using a two-dimensional numerical simulation method in the 'Modeling the thermal structure of the Hikurangi subduction zone' section, and although the uncertainty is large, we conclude that thermal structure also varies along strike. Comparing the estimated thermal models with tectonic tremor and SSE distribution, we conclude that the along-strike variation of temperature on the plate interface can control the along-strike differences in tectonic tremor depth and the down-dip limit of SSEs, mainly by the calculated lateral change in depth of the 600°C isotherm (i.e., the location of the brittle-ductile transition). The depth of the coupling transition, obtained by GPS, can also be explained by the lateral variation of the 350°C isotherm (i.e., the isotherm below which some slab minerals become ductile).

Tectonic setting

In the Hikurangi subduction zone, off the North Island of New Zealand (Figure 1), the Pacific Plate (PAC) is subducting beneath the Australian Plate (AUS). The age of the PAC in this region is estimated to be 120 Ma (Taylor, 2006), and subduction appears to have started at 24 Ma (Ballance 1976; Rait et al. 1991; Kamp, 1999). Because of the complicated nature of the regional tectonic setting, some important physical properties and environmental conditions are known to change significantly along strike in this subduction zone, which are briefly explained below (a thorough review of these along-strike variations is provided by Wallace et al. (2009)).

The first such factor is the convergence rate. The average convergence velocity of the PAC with respect to the AUS along the Hikurangi Trench is about 4.5 cm/year in a direction oblique to the trench axis (Figure 1). However, clockwise block rotation of the upper plate (i.e., AUS) in the forearc region is also known to occur (Wallace et al. 2004; Nicol and Wallace 2007). The orthogonal convergence rate between the PAC and the AUS is higher (approximately 6 cm/year) than the average rate (4.5 cm/year) at the northern end of the Hikurangi Trench and lower (approximately 2 cm/year) than the average rate at the southern end due to this clockwise rotation of the AUS (Figure 1).

The degree of seismic coupling of the plate interface, as estimated from GPS, also changes along strike in the Hikurangi subduction zone (Wallace and Beavan 2010). Seismic coupling transition occurs at very shallow depths (approximately 10 km) in the northern region, but it shifts drastically in the center of the island and occurs at greater depths (approximately 30 km) in the southern region. The down-dip limit of SSEs (Wallace and Beavan 2010; Wallace and Eberhart-Phillips 2013) and tectonic tremors (Fry et al. 2011; Kim et al. 2011; Ide 2012) show similar spatial variations. Deep (approximately 50 km), long duration (approximately 1 year) SSEs have been detected in the transition zone of the southern and central parts of the Hikurangi subduction zone (Wallace and Beavan 2010). Tectonic tremors have also been detected at the central part (Fry et al. 2011; Ide 2012). However, the temporal relationships between SSEs and tectonic tremors remain unclear. Shallow (approximately 10 km), short duration (approximately 1 week) SSEs have also been detected in the coupled zone of the southern part (Wallace et al. 2012). Here, earthquake swarms have accompanied these SSEs (Wallace et al. 2012). Meanwhile, in the northern region of the Hikurangi subduction zone, shallow (approximately 20 km), short duration (approximately 1 week) SSEs occur along narrow zones
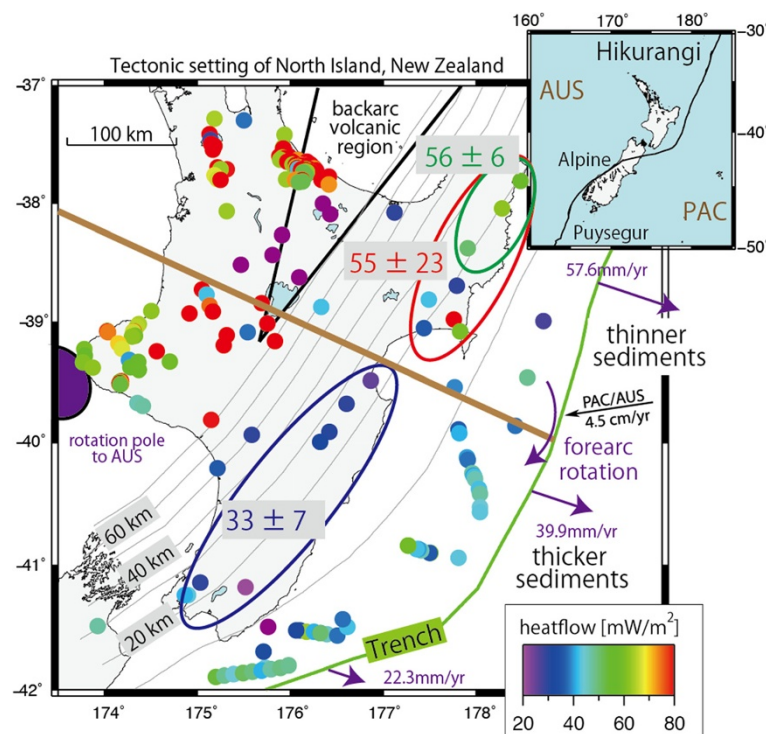
Figure 1 Tectonic setting of the North Island of New Zealand. An overview of New Zealand is shown at the top right, along with the plate boundary between the AUS and PAC. In the main figure, the black arrow shows the plate velocity of the PAC relative to the AUS, and the purple arrows show the orthogonal convergence rates when accounting for the clockwise block rotation of the forearc region (Wallace et al. 2004; Nicol and Wallace 2007). The purple ellipse shows the pole location used for the block rotation. Gray lines represent the plate contours by Ansell and Bannister (1996). The brown line demarcates the location of the cross section used in numerical modeling of the thermal structure. Note that the wedge-shaped volcanic region is also shown. Colored dots represent the observed heat flow data (Global Heat Flow Database compiled by Pollack et al. 1993 and Townend 1997; Allis et al. 1998). Color scale is shown at right bottom of the figure. At three onshore coastal regions (southern, northern, and northernmost coastal region), the mean and standard deviation values of observed heat flow data are indicated.

near the shallowest portion of the uncoupled zone (Wallace and Beavan 2010). Here, both earthquake swarms and tectonic tremors that occur in conjunction with SSEs have also been detected. Earthquake swarms have been located by the slip area of SSEs, while tectonic tremors have been situated around the down-dip edge of the SSE source region (Delahaye et al. 2009; Kim et al. 2011).

The final factor is the along-strike variation in the observed heat flow at the surface. Heat flow at the surface is a direct reflection of the subsurface thermal structure of the underlying crust and mantle. In northern New Zealand, a wedge-shaped volcanic region exists, which is considered to represent the margin of a back-arc extensional event that is laterally continuous with the Kermadec subduction zone to the northeast (Figure 1). In this back-arc volcanic region, heat flow is higher (>100 mW/m^2) than in other places. However, the observed heat flow within the forearc region is lower, and it varies laterally along the plate interface. Although observed heat flow data around onshore coastal region are sparse, it changes as a whole from 33 ± 7 mW/m^2 in the southern region to 56 ± 6 mW/m^2 in the northernmost region (Figure 1,

Global Heat Flow Database compiled by Pollack et al. 1993 and Townend 1997; Allis et al. 1998). Accordingly, some studies have evaluated the thermal structure of the Hikurangi margin based on these observed heat flow data (e.g., McCaffrey et al. 2008; Fagereng and Ellis 2009; Wada and Wang 2009).

Methods and results
Investigation of tectonic tremor events
Data and methods

To detect and locate tectonic tremor events in the Hikurangi subduction zone, we applied the envelope correlation method of Ide (2010, 2012) to continuous velocity seismograms, as described in the next paragraph. The waveforms, originally recorded at 100 samples per second (sps), are downloaded from GeoNet network, which is a local seismic network in New Zealand operated jointly by the Earthquake Commission and GNS Science. We focus on the central part of North Island, where ambient tectonic tremors have been detected previously by Ide (2012).

Twenty-three seismic stations were used from December 2003 to April 2012 to monitor tectonic tremor activity. For

each station, we have prepared two horizontal components of continuous velocity waveforms. The continuous velocity waveforms were band-pass filtered between 2 and 8 Hz, then converted to envelope waveform, low-pass filtered below 0.2 Hz, and then resampled at 2 sps. Continuous envelope data were surveyed using half-overlapping time windows of 300 s. For each time window and each envelope-waveform pair, we calculated cross-correlation coefficients, and if the maximum value of the coefficients exceeded a threshold value of 0.6, we regard the lag time as a travel time difference of S wave. When travel time differences are measured for more than 40 waveform pairs, then we tentatively assumed the occurrence of a seismic event. At this point in the analysis, we would then attempt to locate this event, using the horizontally layered velocity structure proposed by Reyners et al. (2006) (Additional file 1: Table S1). After estimating an approximate epicenter by a grid search, the hypocenter is iteratively estimated so as that squared sum of time residual between observed arrival time differences and synthetic ones is minimized. Once the source location was determined for a given event, we proceeded to stack all envelopes along the synthetic travel time, and we estimated the event duration by the half-value width of the stacked envelope.

This analytical method detected not only tectonic tremors but also ordinary regional earthquakes, relatively large teleseismic earthquakes and many other illusory events that originated from artificial noise. In order to successfully distinguish tectonic tremors from these other types of seismic events, some additional procedures were applied to the detected signals. First, we selected certain events that exhibited a total duration longer than a specified threshold value (50 s). Since tectonic tremor events tend to be visible only in low frequencies, we also investigated the high-frequency components for high-frequency (HF) data sets, which are essentially velocity seismograms that have been band-pass filtered between 10 and 20 Hz, transformed to envelope, and then resampled at 2 sps. For each dataset, if we observed correlation coefficients between HF records higher than a threshold value of 0.6 for more than 40 waveform pairs, we discarded the candidate. Furthermore, we were able to exploit the successive nature of tectonic tremor events by carrying out a clustering procedure on the tectonic tremor candidate catalog, in which we discarded any candidates that were not observed to be associated with any other spatiotemporally synchronous counterpart candidates occurring within at least 0.1 degree of latitude and longitude and 1 day prior or subsequent to the candidate tectonic tremor event in question. We regard these events as tremor candidates.
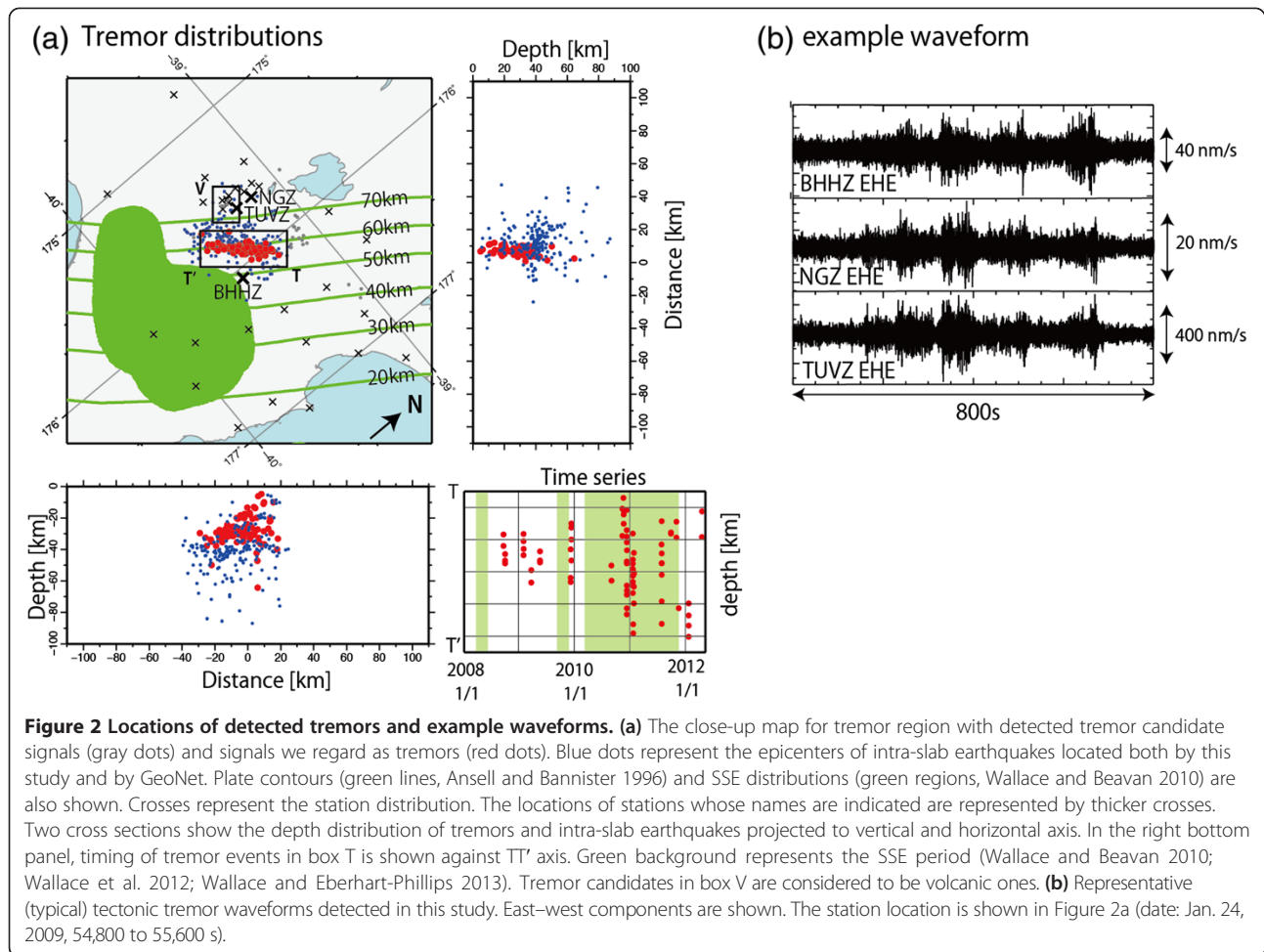
Results of tectonic tremor detection

Figure 2a shows the results of tectonic tremor detection. Although tremor candidates, which include ordinary

earthquakes and misdetections as well, show a pronounced geographic spread (gray dots), there is a discernible cluster aligned NE-SW (box T), which we consider to represent tectonic tremors (red dots). In this region, a total of 84 tectonic tremors were detected. Representative examples of waveforms for these events are shown in Figure 2b. This location is consistent with previously detected tremor (Ide 2012) for older data (2005 to 2009). Another cluster of events (box V) is also found within the back-arc volcanic region, which might be an indication of low-frequency volcanic tremors, which are commonly observed beneath active volcanoes.

To confirm that these signals are of tectonic tremors, not ordinary earthquakes, we have compared the frequency spectrum of these events with that of ordinary earthquakes, having similar epicenters, and that of a distant earthquake (Figure 3). The spectrum of an ordinary earthquake is well fitted by the omega-square model (Brune 1970). If earthquakes are geometrically similar, the corner frequency (fc) is inversely proportional to the cubic root of the seismic moment. Therefore, smaller earthquakes are expected to have a higher corner frequency (Figure 3a). In Figure 3b, an example of a distant earthquake, which cannot be well fitted by omega-square model, is compared with intra-slab earthquakes occurring below tremor sources. The distant earthquake has smaller spectrum amplitude in high-frequency range (>4 Hz) than the intra-slab earthquake, although it has larger amplitude in lower frequency range (<1 Hz).

In Figure 3c, two examples of detected tectonic tremor signals are shown. They exhibit a completely different spectrum from ordinary earthquakes and the distant earthquake, in that the spectrum amplitude in 3 to 10 Hz frequency range is smaller, while their spectrum amplitudes are almost the same in 0.1 to 1 Hz frequency range. In other words, if these signals were actually of regular earthquakes, they should have a higher fc, i.e., because in this case, they exhibit smaller signals than regular earthquakes shown in each figure. Not only is the fc of these signals lower than that for regular earthquakes but also their spectrum cannot be well fitted by the omega-square model. Since we have compared tremors with the intra-slab earthquake, which has a similar epicenter as tremors, the amount of attenuation for tremors and the intra-slab earthquake should not differ drastically. Therefore, we considered that these signals represent signals of *bona fide* tectonic tremor events.

Notably, the location of tremors coincides with the down-dip edge, rather than central area, of known SSE areas (Figure 2a). Tremors are also clustered in time, although there is no evidence of any kind of periodicity (Figure 2a). An especially large tremor burst occurred from the end of 2010 to the beginning of 2011. An SSE occurred at the up-dip region of tremor activity in 2010,

Figure 2 Locations of detected tremors and example waveforms. (a) The close-up map for tremor region with detected tremor candidate signals (gray dots) and signals we regard as tremors (red dots). Blue dots represent the epicenters of intra-slab earthquakes located both by this study and by GeoNet. Plate contours (green lines, Ansell and Bannister 1996) and SSE distributions (green regions, Wallace and Beavan 2010) are also shown. Crosses represent the station distribution. The locations of stations whose names are indicated are represented by thicker crosses. Two cross sections show the depth distribution of tremors and intra-slab earthquakes projected to vertical and horizontal axis. In the right bottom panel, timing of tremor events in box T is shown against TT' axis. Green background represents the SSE period (Wallace and Beavan 2010; Wallace et al. 2012; Wallace and Eberhart-Phillips 2013). Tremor candidates in box V are considered to be volcanic ones. **(b)** Representative (typical) tectonic tremor waveforms detected in this study. East–west components are shown. The station location is shown in Figure 2a (date: Jan. 24, 2009, 54,800 to 55,600 s).

though there is a few months lag between the occurrence of SSE around tremor hypocenters and the activation of tectonic tremor (Bartlow et al. 2014).

Estimation of tectonic tremor depths

The depths of tectonic tremor events documented within the Hikurangi subduction zone have not been well constrained in the previous studies. Here, we provide relatively accurate estimates of the depths of tremor events. Because the absolute tremor depth estimated by envelope correlation method is not accurate, we have estimated the relative depth of tectonic tremors to intra-slab earthquakes. We have also estimated the bias in the depth between our catalog and local GeoNet catalog using intra-slab earthquakes detected both in this study and by GeoNet, since depths of ordinary earthquakes in the GeoNet catalog are probably less biased.

A seismic event detected by our method is assumed to be identical to an intra-slab earthquake in the GeoNet catalog if two origin times in minutes are identical and the two epicentral locations are separated by less than 0.5° in both latitude and longitude. The distribution of

identified intra-slab earthquakes is shown as blue dots in Figure 2a. The depths of these intra-slab events estimated by our method are shallower than the depths in the GeoNet catalog (Figure 4a). This is because our method uses only S wave information, while the routine analysis uses both P and S waves. We confirmed for several selected events that a similar depth with GeoNet catalog was estimated using manually picked P and S arrivals, meanwhile a similar depth with our catalog by the envelope correlation method was estimated when only manually picked S arrivals were used. Hence, we believe that these biases seen in Figure 4a are inherent in the method.

Nevertheless, we consider the relative depths of tectonic tremor versus intra-slab seismic events to be less biased. Figure 4b shows the differences in depth distribution between tectonic tremors and intra-slab earthquakes, estimated by our method. Overall, the depths of tectonic tremors are shallower by about 15 km than the depths of intra-slab earthquakes. Since the depths of intra-slab earthquakes are about 60 to 65 km in this region, as determined by the routine analysis, we can infer
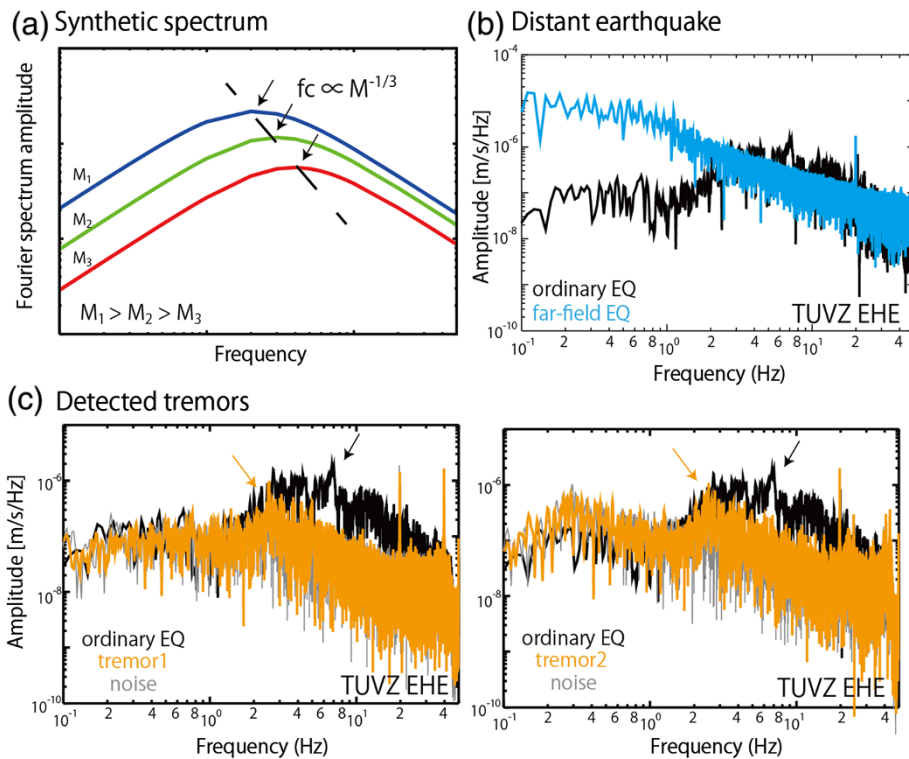
Figure 3 Comparison of the velocity spectrum between ordinary earthquake, tectonic tremor and noise. (a) Synthetic velocity power spectrum of the omega-square model (Brune 1970). Arrows show the corner frequency, corresponding to the peak of spectra. **(b)** Comparison of velocity power spectra between an ordinary intra-slab earthquake and a distant earthquake at station TUVZ (Figure 2a). **(c)** Comparison of velocity power spectra between an ordinary intra-slab earthquake and two examples of tectonic tremors, all of which occurred with similar epicenter. Black arrow represents the peak of spectrum (approximate corner frequency) of the ordinary earthquake. Orange arrow represents the peak of tectonic tremor spectrum. Date, time, and location of events: ordinary earthquake for **(b)** and **(c)**: May. 2, 2009, 52,230 to 52,270 s (39.46°S, 175.83°E, 54 km in GeoNet catalog); distant earthquake for **(b)**: Sep. 8, 2010, 42,130 to 42,160 s (20.52°S, 170.06°N, 14.1 km in Global CMT catalog; Dziewonski et al. 1981; Ekström et al. 2012); tectonic tremor 1 for **(c)**: Jan. 24, 2009, 53,350 to 53,450 s (39.36°S, 175.93°E, 23.9 km in this study); tectonic tremor 2 for **(c)**: May. 12, 2009, 26,200 to 26,300 s (39.39°S, 176.00°E, 33.4 km in this study).
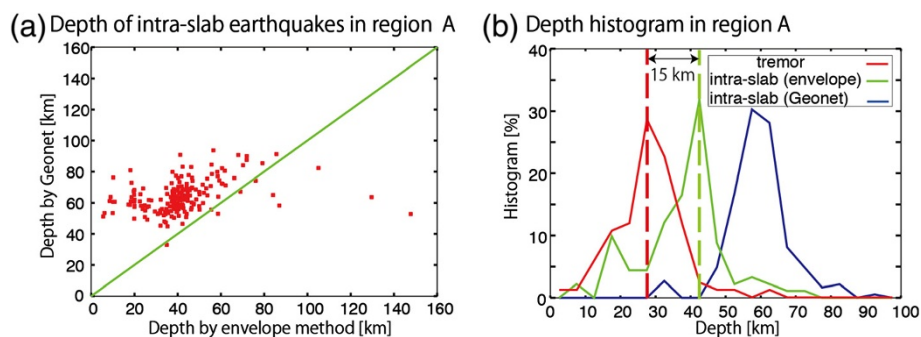

Figure 4 Depths of tectonic tremors and intra-slab earthquakes. (a) Comparison of estimated depths of intra-slab earthquakes determined by the GeoNet method versus our method. On the green line, depths estimated by the two methods are equal. Our method tends to estimate shallower depths. **(b)** Depth histogram of intra-slab earthquakes and tectonic tremors. The red line shows depth histogram of tectonic tremors estimated by our method, while the green line shows intra-slab earthquakes. The blue shows intra-slab earthquakes estimated by the GeoNet. Tectonic tremors are about 15 km shallower than intra-slab earthquakes.

that the depths of tectonic tremor events are about 45 to 50 km, assuming that the relative depths are not biased. These depths seem to be close to the depth of the plate boundary in this region. We will discuss this point again in the 'Relationship between tectonic tremors and the plate interface' section.

Modeling the thermal structure of the Hikurangi subduction zone
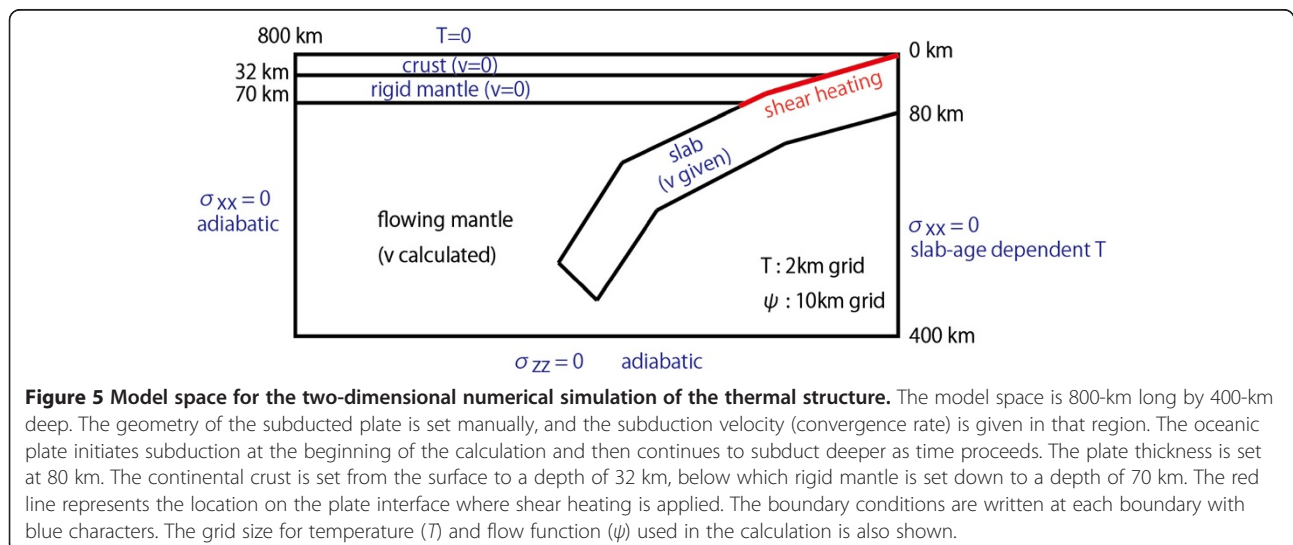
Thermal modeling methods

We calculated the thermal structure of the Hikurangi subduction zone using the two-dimensional finite difference code developed by Yoshioka and Sanshadokoro (2002) and Torii and Yoshioka (2007), in which the equations for momentum (inertial term is neglected) and energy are solved simultaneously as a coupled problem with viscous dissipation and adiabatic heating. In addition, we use frictional heating and radiogenic heating (following Yoshioka et al. 2013) to accurately obtain the temperature distribution in the whole model space. We present a brief description of our calculations below, and more details are given in the Appendix.

Figure 5 shows a schematic model space for the Hikurangi subduction zone. In its entirety, the model space measures 800 km in length and 400 km in depth. This size is large enough to encompass our entire region of interest (i.e., the plate interface where tectonic tremors are considered to occur). The continental crust, which has a thickness of 32 km in average beneath the North Island of New Zealand, combined with the upper mantle above 70 km depth, is considered in this model to effectively represent the continental lithosphere, which itself is treated as a conductive layer. The geometry of the subducted slab (Figure 5), along the brown line shown in Figure 1, is constructed based on the slab model of

Ansell and Bannister (1996) and used for all calculations because the slab shape does not change drastically in the along-strike direction (Figure 1). Subduction is considered to start at the beginning of the calculation (24 Ma), after which the oceanic plate subducts gradually at a constant rate till the end of the calculation (the present) at time increments of about 0.071 m.y. for the lowest subducting velocity (2 cm/year) in the southern region and about 0.024 m.y. for the fastest subducting velocity (6 cm/year) in the northern region.

The mantle surrounding the slab below 70 km represents a free-flowing region, where the momentum equation is solved. We used this depth of 70 km so that the calculated heat flow around the tip of the mantle wedge in the central transition zone should reproduce the observed one. Since the calculated surface heat flow around the tip of the mantle wedge is increased by including the effect of the free-flowing mantle, its effect is also essential when estimating the temperature along the plate interface. Zero normal stress is assumed as a boundary condition for the momentum equation at both the sides and the bottom of the model region. Zero motion is assumed at the top boundary, where landward free-flowing regions contact with the upper rigid lithosphere. We put the value of the stream function, calculated from the velocity of the subducting slab and its direction, in the region where the slab exists to express the movement of the slab.

The thermal boundary condition is set to a constant 0°C at the top of the model region. The temperature boundary conditions on the left side and the bottom of the model region are adiabatic. The boundary conditions on the right side of the model region are fixed by a variable temperature profile that is directly dependent on the age of the slab; the profile was calculated following the method of Stein and Stein (1992). In addition, for the entire duration of

Figure 5 Model space for the two-dimensional numerical simulation of the thermal structure. The model space is 800-km long by 400-km deep. The geometry of the subducted plate is set manually, and the subduction velocity (convergence rate) is given in that region. The oceanic plate initiates subduction at the beginning of the calculation and then continues to subduct deeper as time proceeds. The plate thickness is set at 80 km. The continental crust is set from the surface to a depth of 32 km, below which rigid mantle is set down to a depth of 70 km. The red line represents the location on the plate interface where shear heating is applied. The boundary conditions are written at each boundary with blue characters. The grid size for temperature (T) and flow function (ψ) used in the calculation is also shown.

the model calculations, a fixed slab age of 80 Ma was used, and this corresponds to the same age assumption made by McCaffrey et al. (2008). Although the actual age of the subducted plate must have changed from the start of subduction to the present day, it would nevertheless be sufficiently old not to change the thermal state of the incoming plate very much (Stein and Stein 1992).

At the start of subduction in our thermal modeling study, the distribution of temperature is given as a stratified temperature profile, which is constrained by carrying out a half-space cooling calculation on 1,350°C homogeneous mantle for 20 m.y., and we assume adiabatic compression. The initial continental age is estimated on the basis of heat flow in the back-arc region, so that our modeling results are roughly consistent with the observed heat flow in this area. This parameter has no influence on the temperature in our region of interest because the temperature in the forearc region is mostly controlled by shear heating and the advection of the slab.

Frictional heating is calculated in the brittle region of the plate interface using the methods of Byerlee (1978) and in the ductile region using the flow law for diabase presented by Caristan (1982) (Appendix). Distinguishing whether a calculation point is in the brittle or ductile region is done automatically, by assuming that the brittle-ductile transition is defined as the depth at which shear strain in the ductile deformation regime becomes smaller than that found in the brittle deformation regime. Frictional heat is considered to be the product of both shear stress and strain rate on the plate interface. In addition, a high frictional parameter (a frictional parameter of pore pressure ratio $\lambda \sim 0.95$) reduces the effective normal stress, thus also reducing shear stress and shear heat in the brittle deformation regime (see Appendix for details). In this

model, all kinds of effects that lead to an increase or decrease in shear heat are included in this λ. Furthermore, we applied frictional heating to the plate interface over a depth range of 0 (at the surface) to 70 km. On the deeper plate interface, slip-weakening behavior with cutoff velocity is sometimes assumed to reproduce SSE in the simulation study (e.g., Shibazaki et al. 2012), which is based on the experimental study of Shimamoto (1986, 1989). Hence, we consider that frictional heating can be applied to deeper plate interface as well.

Temperature distributions along three profiles

As described in the 'Tectonic setting' section, the observed heat flow data at onshore coastal region varies along strike. In the southern and central coast, observed heat flow value is low (33 ± 7 mW/m^2), while it is higher (56 ± 6 mW/m^2) in the northernmost coastal region (Figure 1). To reproduce this along-strike variation pattern of the observed heat flow data at onshore coastal region, we carried out a series of numerical simulations that incorporated the variations in convergence rate and frictional parameter (λ). In making these calculations, we assigned three values to each parameter for nine possible scenarios. With regard to the convergence rates used in these numerical simulations, a value of 6 cm/year for the northern region was used to represent relatively fast subduction, whereas progressively slower rates of 4 and 2 cm/year were assigned to the central and southern regions, respectively (after Wallace et al. 2004). Three values (0.94, 0.96, and 0.98) were used for λ.

Figure 6 shows the calculated heat flow in southern and northern part of the subduction zone for three λ values with heat flow data observed at regions in the southwestward and northeastward strike direction from
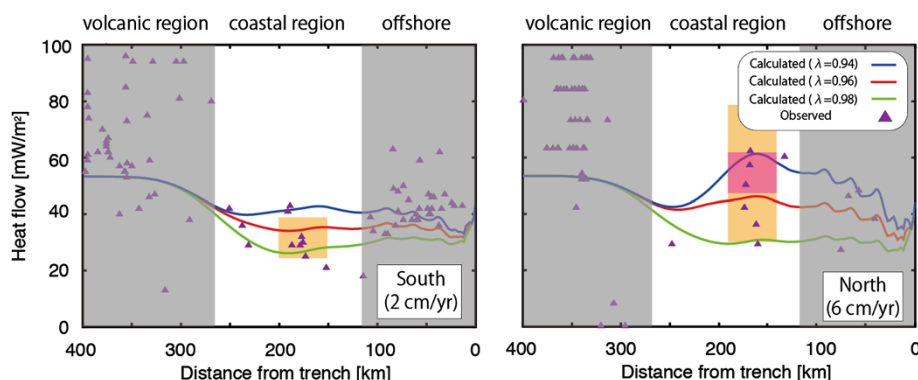

Figure 6 Observed and calculated heat flow in the southern and northern regions. Thermal structure is calculated with 2 and 6 cm/year convergence rate for southern and northern regions, respectively. Three values of frictional parameter (λ =0.94, 0.96, and 0.98) are tested in each region, which are represented by blue, red, and green lines, respectively. Triangles indicate observed heat flow values. Heat flow values observed at regions in the southwestward and northeastward strike direction from the brown line in Figure 1 are shown in South and North panel, respectively. Shaded area represents the volcanic region, which is not considered in our model, and offshore region, where the observed heat flow data have large uncertainty. Two orange-colored rectangles and a magenta-colored rectangle show the mean and standard deviation values of observed heat flow data at southern, northern, and northernmost onshore coastal region, respectively (Figure 1).

the brown line in Figure 1, respectively. In the southern part, higher λ value (0.96 to 0.98, i.e., smaller frictional heating) is required to reproduce lower heat flow at coastal region. Although observed heat flow is higher than calculated one at near-trench region here, these off-shore data are obtained using the depth to a gas hydrate related bottom simulating reflector, which is considered to have relatively large uncertainty. Hence, we give more importance to heat flow observation at on-shore coastal region. Meanwhile, in northern part, though the scatter of observed heat flow data is large, lower λ value (0.94 to 0.96, i.e., larger frictional heating) is required to explain higher heat flow at northernmost coastal region. These comparisons suggest that frictional parameter λ should vary in the strike direction from about 0.98 at southern part, where convergence rate is 2 cm/year, to about 0.94 at northernmost part, where convergence rate is 6 cm/year, through the transitional part with medium value (0.96), where convergence rate is 4 cm/year. Thermal and stress profile on the subducting plate interface calculated for these three sets of parameters are shown in Figure 7.

This along-strike change of frictional parameter might be related to the along-strike change of sediment thickness in the trench because the amount of sediment might have influenced on the amount of pore fluid (Clift and Vannucchi 2004; van Keken et al. 2011). In the Hikurangi subduction zone, it is known that the thickness of turbidite sequence at the trench varies drastically in the along-strike direction, from thicker (typically approximately 3 km, approximately 6 km at most) in the south to thinner (approximately 1 km) in the north (Lewis et al. 1998; Wallace et al. 2009). Although the difference of sediment thickness might change the temperature at trench by about 50°C,

which may change the brittle-ductile transition depth by approximately 5 km, it is not significant compared to the much bigger along-strike difference (Figure 7).

Figure 7 shows three numerically modeled profiles displaying temperature and shear stress along the plate interface considering the aforementioned along-strike variation of convergence rate and frictional parameter. In these profiles, the shear stress increases with depth at shallower part due to the brittle behavior of plate interface. At this frictional regime, the temperature on the plate interface also increases rapidly with depth. The shear stress value exhibits a maximum when frictional behavior transits from brittle one to ductile one, and then it decrease with depth below the transition depth. The temperature on the plate interface increases more slowly in this regime. This indicates that the temperature gradient is dependent on the deforming regime. Because of the along-strike variation of convergence rate and frictional parameter, the depth of the brittle-ductile transition varies from about 60 km in the southern region (calculated with λ =0.98 and 2 cm/year) to about 25 km in the northern region (calculated with λ =0.94 and 6 cm/year).

By comparing numerical models for the nine scenarios, we can examine the relative stability or variability of temperature, as estimated for different regions of the plate interface (Figure 8). In deeper regions (approximately 50 km), the model temperature is 600°C for all parameter sets except those which were assigned with the highest values of λ (i.e., 0.98). In contrast, in shallower regions (approximately 20 km), the model temperatures vary according to the differing values of λ and convergence rate, although we also note that there is probably an additional trade-off between shear heating and advective cooling, which has not been investigated
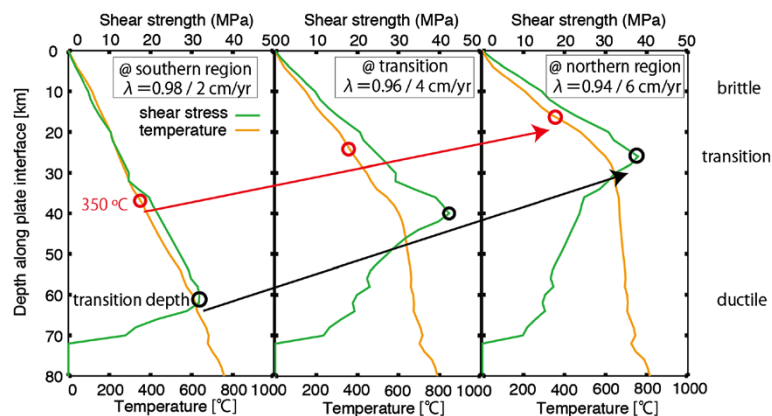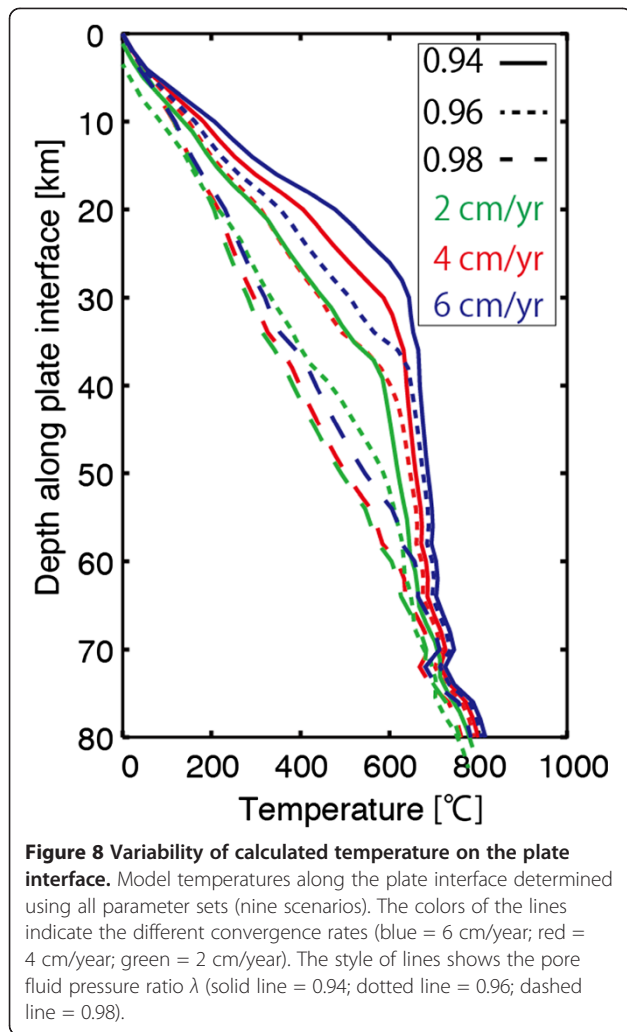

Figure 7 Along-strike comparison of the results of numerical simulation of the thermal structure. Along-strike variation in temperature and shear stress on the plate interface is shown. The green lines indicate shear stress, while the orange lines indicate temperature. These values are calculated with (λ, convergence rate) = (0.98, 2 cm/year) for southern region (left panel), (0.96, 4 cm/year) for transition (middle panel), and (0.94, 6 cm/year) for northern region (right panel). The black circles show the depth of the transition from a brittle deformational regime to a ductile one, and the red circles show the depth where the temperature is 350°C.

Figure 8 Variability of calculated temperature on the plate interface. Model temperatures along the plate interface determined using all parameter sets (nine scenarios). The colors of the lines indicate the different convergence rates (blue = 6 cm/year; red = 4 cm/year; green = 2 cm/year). The style of lines shows the pore fluid pressure ratio λ (solid line = 0.94; dotted line = 0.96; dashed line = 0.98).

(see the 'Estimation of tectonic tremor depths' section) should coincide with the depth of the plate boundary, as estimated in the previous studies. To date, a number of models have been proposed for the plate geometry within the Hikurangi subduction zone, constrained using various techniques. For instance, Ansell and Bannister (1996) estimated the location of the plate boundary using the seismicity of ordinary earthquakes, whereas Bannister et al. (2007) constrained the plate geometry within the central part of the subduction zone by analyzing receiver functions; of note, the depth of the latter plate boundary is slightly shallower than that of the former.

In the central part of North Island, depths estimated for the plate interface beneath the tremor epicenters are either about 55 km (Ansell and Bannister 1996; Williams et al. 2013) or 45 to 50 km (Bannister et al. 2007). The latter depth coincides approximately with our estimate for the depth of tectonic tremor events. This coincidence is not surprising because the results of receiver function analysis are considered to be more accurate when estimating the location of a sharp structural change like the plate interface. Although the apparent vertical separation between tectonic tremor events (i.e., the plate interface) and intra-slab earthquakes seems to be slightly too large (approximately 15 km; Figure 4b) when compared with the typical separation of about 10 km in other subduction zones (Shelly et al. 2006; Yabe and Ide 2013), the discrepancy might reflect the thick oceanic crust of the subducted Hikurangi Plateau. Therefore, we can conclude that tectonic tremor events do actually seem to occur around the plate interface in this region of the Hikurangi subduction zone.

Comparisons with thermal structures deduced in the previous studies

As we showed in the 'Temperature distributions along three profiles' section, variations in the along-strike thermal structure are needed to explain along-strike variations of the observed heat flow within the Hikurangi subduction zone. This challenges the idea put forth by McCaffrey et al. (2008), who suggested that the thermal structure across this subduction zone does not vary along strike. They used an approximation made with a simple equation developed by Molnar and England (1995), and although they were able to sufficiently explain the offshore heat flow data, they were not able to provide an adequate explanation of the inland heat flow data measured in the onshore coastal region (Figure 1).

Fagereng and Ellis (2009) also concluded that the variation in thermal structure along the Hikurangi subduction zone is small, and they suggested that the along-strike variation in seismic coupling is mainly due to differences in local pore fluid pressures and convergence rates. However, they did not reproduce the higher heat flow values

in detail in our study. For the tectonic tremor region near the central part (or northern edge of southern part) of the North Island (Figure 2a), the modeled temperatures are very high (at least 500°C even for the highest corresponding λ parameter) for the scenarios set to a convergence rate of 2 and 4 cm/year. On the other hand, in the northern region, although the model temperatures determined at tectonic tremor depth vary from 250°C to 500°C in response to variations in the value of λ for the scenarios set to a convergence rate of 6 cm/year, higher temperature model (i.e., lower λ model) is appropriate in the light of the observed higher heat flow at onshore coastal region.

Discussion

Relationship between tectonic tremors and the plate interface

Because tectonic tremors are thought to represent shear slip along the plate interface (Ide et al. 2007; Shelly et al. 2007a), the estimated depths of tectonic tremor events

observed in the northern region. Although our idea is similar to theirs, our numerical simulations do not require the same large differences in λ that Fagereng and Ellis (2009) used (0.4 to 0.95 for a linear plate interface geometry) to reproduce the observed along-strike variations in heat flow. Such a drastic change of pore fluid pressure along the strike of this subduction zone might be unrealistic because Seno (2009) indicated that pore fluid pressures within subduction zones worldwide, including those where very old oceanic plate is being subducted, are always very high, regardless of the age of the subducted plate. It is important to highlight at this point that our calculations also take into account several additional realistic and presumably very important effects such as mantle flow, the bent-plate geometry, as well as the relatively small frictional parameter changes that take place from one region to another along the trench. Because of mantle flow in the mantle wedge, the plate geometry affects both the distribution of frictional heating along the plate interface and the calculated peak of heat flow, and this consequently affects the estimation of temperatures along the plate interface.

Wada and Wang (2009) also calculated the thermal structure of the Hikurangi subduction zone, but they did not address the possibility of any significant along-strike variation in the thermal structure on the plate interface. According to their results, the overall temperature for the Hikurangi subduction zone is lower than that estimated in our numerical modeling and in the previous studies. They did reproduce the heat flow at the surface without having to invoke a large amount of frictional heating, but this contrasts with our model where frictional heating is a necessary condition for producing the observed heat flow above the subduction zone.

One problem is that the literature contains numerous estimates of the temperature along the plate interface in the Hikurangi subduction zone, and the results are inconsistent with each other. For example, the temperature at about 50 km depth was estimated to be around 200°C to 250°C by Wada and Wang (2009), 350°C to 400°C by Fagereng and Ellis (2009), around 400°C to 450°C by McCaffrey et al. (2008), and around 600°C in the present study. Although accurate and precise values of temperature along the plate interface in the Hikurangi subduction zone may not yet be well constrained, we nevertheless think that we can conduct relative comparisons between some of the important parameter sets (scenarios) in a self-consistent model, and the results should provide along-strike variations in the thermal structure of the Hikurangi subduction zone.

Previous studies of the Hikurangi subduction zone have involved two-dimensional models, and our investigation is no different in that respect. Nevertheless, our conclusions differ from those of the previous studies in a number of important ways, such as along-strike variation of thermal structure and the temperature around tremor source region. Furthermore, Reyners et al. (2006) pointed to the three-dimensional mantle flow in the Hikurangi subduction zone, where flow is from south to north, parallel to the trench, and the effects of that flow are beyond the calculations of any of the two-dimensional models. However, this effect should be to weaken the along-strike variations, and we do consider that here, thereby helping us to estimate the upper limit of the along-strike variation with our two-dimensional model.

Relationship between thermal structure and tectonic tremor events

Table 1 summarizes the observed along-strike variations in depth of some key characteristics of the Hikurangi subduction zone pertaining to the calculated thermal structure, estimated depth of tectonic tremor events, the distributions of SSEs, the seismic coupling transition depth, and the calculated location of the brittle-ductile transition. Notably, our calculated depths for the brittle-ductile transition coincide closely with both the observed depths of tectonic tremor events (this study) and the down-dip limit of SSEs. In addition, the estimated seismic coupling transition depths are similar to those estimated for the 350°C isotherm. The calculated brittle-ductile transition depth is quite consistently at depths

Table 1 Summary of along-strike variations in seismic characteristics and thermal structure calculated during this study

Feature	South	(Central transition)	North
Tremor	-	45 to 50 km	(Approximately 20 km)
SSE	5 to 15 km	10 to 15 km	10 to 20 km
	30 to 50 km	20 to 60 km	
Seismic coupling transition	Approximately 30 km	Approximately 10 km/approximately 30 km	Approximately 10 km
350°C	Approximately 35 km	Approximately 25 km	Approximately 15 km
Brittle-ductile transition (approximately 600°C)	Approximately 60 km	Approximately 40 km	Approximately 25 km

Tectonic tremor depth at central part was determined during this study. In the northern part, the depth of plate interface where tremors are detected by Kim et al. (2011) is about 20 km in the plate model of Ansell and Bannister (1996). The depth of SSE is from Wallace et al. (2004, 2012), Wallace and Beavan (2010), and Wallace and Eberhart-Phillips (2013). The depth of seismic coupling transition is based on Wallace and Beavan (2010). The 350°C depths (isotherm) along with the locations (depths) of the brittle-ductile transition were calculated during this study, as shown in Figure 7.

where the temperature is around 600°C because the amount of ductile shear stress acting on the rocks rapidly decreases at this temperature to comparatively low values with respect to the amount of brittle shear stress, as would be expected when moving into a completely ductile regime. At depths where the temperature is 350°C, the brittle-ductile transition has taken place for some rock-forming minerals. This means that transitional slip behavior starts at such depths, which results in the genesis of tectonic tremors rather than ordinary earthquakes between 350°C to 600°C. In contrast, SSEs distribution (Wallace and Beavan 2010; Wallace et al. 2012; Wallace and Eberhart-Phillips 2013) seems to be able to exist even where temperature on the plate interface is low. This would be possible because SSEs are observed not only around tremor source region but also in any other places around ordinary earthquake regions (e.g., Kato et al. 2012; Ito et al. 2013). In summary, in a very brittle regime at shallow depths, complete seismic coupling causes ordinary earthquakes and earthquake swarms with SSE; in the brittle-ductile transitional zone, insufficient coupling is exhibited, and tectonic tremor with SSE occurs between 350°C to 600°C and tectonic tremor events are mainly situated near the bottom of this transitional area, at around 600°C (Table 1). At deep depth where temperature is above 600°C, only stable slip occurs. This accordance suggests that the slip behavior on the plate interface, such as tectonic tremor events and the down-dip limit of SSEs, are mainly controlled by temperature. The absolute values of the temperature at the starting point of the partial ductile regime (350°C) and the more complete brittle-ductile transition (600°C), as outlined in this study (Table 1), might have some biases as discussed in the 'Comparisons with thermal structures deduced in the previous studies' section. The important thing to highlight here is that, ostensibly, there are two significant boundaries represented: one corresponding to the start of partial rock ductility and the other corresponding to the transition from unstable slip to a more stable form of ductile deformation. The absolute temperatures of those transitions might vary among subduction zones according to their specific tectonic environment, the variations in the total thickness of the subducted sediments, and/or the composition of the subducted sediments. This idea is illustrated in Figure 9.

By comparing the estimated values of temperature in the vicinity of the source regions for tectonic tremors among three different subduction zones, Brown et al. (2009) proposed that tectonic tremors are not simply controlled by temperature alone. However, it is important to note that the comparisons in their study were based on thermal models constrained by various authors that presumably employed different strategies/techniques in constructing their own individual models of the thermal structure of those various subduction zones. Accordingly,
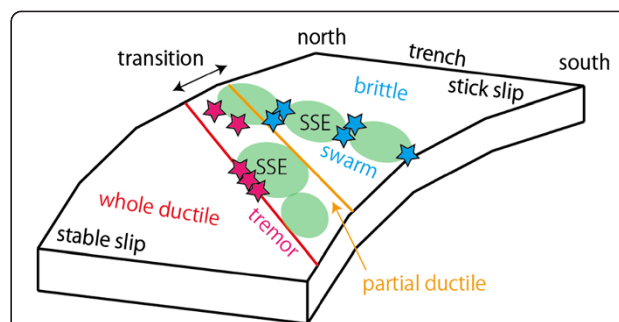

Figure 9 Schematic figure showing the relationship between seismicity and temperature. In the shallower region, the temperature is low and ordinary earthquakes occur (stick–slip behavior). At depths where temperature reaches 350°C (orange line), some minerals start to deform in a ductile manner, and seismic coupling weakens. Below the depth where temperature exceeds 600°C (red line), the entire rock deforms in a ductile manner (stable slip), and neither earthquakes nor tectonic tremors occur. Tectonic tremors occur at locations where temperatures are around 600°C, just before stable slip takes over with depth.

since the calculation of thermal structure in subduction zones requires several different assumptions, making comparisons between different models for different subduction zones is inherently a tricky problem, as we have seen when making comparisons between our work and the previous studies on the Hikurangi subduction zone (e.g., in the 'Comparisons with thermal structures deduced in the previous studies' section).

Peacock (2009) calculated the thermal structure for the Nankai and Cascadia subduction zones and concluded that tectonic tremors are not controlled by a specific temperature. This particular study used a consistent model for comparing the two subduction zones; however, one cannot necessarily assume that tectonic tremors will occur at the same temperature in all subduction zones because there may be other specific environmental differences between them that are important in terms of modeling their individual thermal structures. To circumvent this problem, we have modeled and examined the along-strike variations in thermal structure within one single subduction zone, and variations in the tectonic environment did not play an important role, therefore implying that any effects of temperature on the generation of tectonic tremor events should in our case be seen more clearly. In the light of this, our conclusion that the generation of tectonic tremor events can be temperature-dependent should be quite valid, at least in the case of our study on the Hikurangi subduction zone.

Conclusions

We have documented several parameters for the Hikurangi subduction zone of northern New Zealand that seem to vary systematically along the strike of the plate interface. These include the convergence rate, the thickness of

sediments, seismicity, seismic coupling, and SSEs. By using continuous seismogram records obtained from GeoNet, we have confirmed the existence of tectonic tremors in the central part of the North Island documented in the previous studies. In addition, we have constrained their depths relative to the plate interface through comparisons with ordinary intra-slab earthquakes.

We also modeled the thermal structure of the Hikurangi subduction zone along a vertical profile oriented perpendicularly to the strike direction of the plate interface, and for this model, we considered the known along-strike variations in convergence rates. To reproduce the along-strike variations of observed heat flows, especially at onshore coastal region, we needed to use along-strike variations in the pore pressure ratio related to interplate friction.

We have compared the estimated thermal model with the along-strike variations in tectonic tremor, SSE, and seismic coupling transition depth. The depth of the brittle-ductile transition on the plate interface in these numerical models coincides closely with the estimated depths of tectonic tremors and the down-dip limit of SSEs. Furthermore, the observed along-strike variations in seismic coupling transition can also be explained by the lateral change in depth of the 350°C isotherm on the plate interface, at which depth the rheology of some common minerals in this environment would begin to exhibit partially ductile behavior. The brittle-ductile transition is thought to be controlled mainly by temperature, which means by inference that the occurrence of tectonic tremors is also mostly dependent on temperature. Consequently, as there are many different factors controlling the temperature, and these factors may differ significantly among different subduction zones, comparisons of tectonic tremor activity and thermal profiles in parts of a single subduction zone are more efficient in terms of evaluating the possible dependency of tectonic tremor activity on temperature.

Appendix

The fundamental equations for our thermal calculations, the momentum equation, and the energy equation, are based on Yoshioka and Sanshadokoro (2002) and Torii and Yoshioka (2007).

$$\frac{\partial^2}{\partial x \partial z}\left[4\eta \frac{\partial^2 \psi}{\partial x \partial z}\right] + \left(\frac{\partial^2}{\partial z^2} - \frac{\partial^2}{\partial x^2}\right)\left[\eta\left(\frac{\partial^2}{\partial z^2} - \frac{\partial^2}{\partial x^2}\right)\psi\right] = \frac{\partial}{\partial x}\left(\rho_0 g \alpha T\right)$$

$$pC_p\left(\frac{\partial T}{\partial t} + \vec{v}\cdot \nabla T\right)$$
$$= k\nabla^2 T + v\rho_0 g \alpha T + 4\eta\left(\frac{\partial^2 \psi}{\partial x \partial z}\right)^2$$
$$+ \eta\left(\frac{\partial^2 \psi}{\partial z^2} - \frac{\partial^2 \psi}{\partial x^2}\right)^2$$
$$+ H_0 \exp\left[-\frac{z}{10}\right] + \frac{\tau v_{pl}}{w}$$

The consideration of radioactive heating and frictional heating (the last two terms in energy equation) are based on Yoshioka et al. (2013). Here, ψ and T represent a stream function and temperature, respectively. $\vec{v} = (u, v)$ is the velocity vector, k is thermal conductivity, C_p is a constant pressure specific heat, g is a gravity constant, and ρ is density, which depends on temperature following Andrews (1972) with a thermal expansivity of α.

$$\rho = \rho_0(1 - \alpha T)$$

H_0 is a radioactive heating constant. Radioactive heating decays with depth following Furukawa (1995). η is the viscosity of flowing mantle calculated following Burkett and Billen (2010) at the estimated upper and lower limits of mantle viscosity of 10^{23} and 10^{20} Pa·s, respectively. The values of constant parameters are listed on Additional file 1: Table S2.

The last term in the energy equation represents shear heating along the plate interface, which is applied to the plate interface from the surface to 70-km depth. τ represents shear stress along the plate interface. It is determined by the following procedure: first, for one point on the plate interface, we have the pressure and temperature on that point, and then we calculate brittle and ductile shear stresses using Byerlee (1978) and Caristan (1982), respectively.

$$\tau_{\text{brittle}} = 0.85\sigma_n(1-\lambda) \quad (\sigma_n(1-\lambda) \leq 200 \text{ MPa})$$

$$\tau_{\text{brittle}} = 50 + 0.60\sigma_n(1-\lambda) \quad (\sigma_n(1-\lambda) \geq 200 \text{ MPa})$$

$$\tau_{\text{ductile}} = \frac{1}{2}A^{-\frac{1}{n}}\dot{\in}^{\frac{1}{n}}\exp\left[\frac{E}{nRT}\right]$$

We adopt the smaller one for an appropriate value in our calculation. We can automatically obtain the brittle-ductile transition depth, which depends on the temperature profile along the plate interface at that time, using this procedure. Here, σ_n is the normal stress, though we use pressure instead. λ is usually interpreted as pore fluid pressure. However, in this study, we call this parameter the 'frictional parameter' because this parameter includes all effects that reduce or increase frictional heating along the plate interface, such as strength weakening during coseismic slip or cooling by the flow of fluids along the plate interface. A is a constant, n is a stress factor, E is the activation energy, and R is the gas constant. These parameters are also listed on Additional file 1: Table S2. $\dot{\in}$ is the strain rate, which is obtained by dividing plate velocity by thermal dissipation length. Frictional heating is obtained by multiplying shear stress τ and the plate velocity v_{pl}. However, to calculate frictional heat in the energy equation, we have to convert it from heat per area to heat per volume. We divided the frictional heat by the thermal dissipation length w, which we assume to be 2,000 m.

The whole model space is 800 km (horizontal) × 400 km (vertical). As an initial condition with no slab, there is a stratified temperature profile which is constrained by carrying out a half-space cooling calculation of 1,350°C homogeneous mantle for 20 m.y., and we assume adiabatic compression. With increments of time, the slab subducts from the right boundary through the passage, which is constrained by the present geometry of the slab. The top 70 km is set as a conductive layer (i.e., continental lithosphere), which is made up by 32-km crust and upper mantle. The mantle, which is not conductive, is considered to be free-flowing, with the movement obtained by solving the momentum equation. At the side and bottom boundaries, zero normal stress is given. At the top boundary, a rigid condition is given on the landward boundary. The value of the stream function is given following the velocity and direction of the subducted slab. We first solve the momentum equation with a 10-km grid. Because the inertial term is neglected in the momentum equation, we can solve it as a simple inverse problem at each time step. Then, we interpolate the stream function into a 2-km grid and solve the energy equation. As for the boundary condition of the energy equation, the adiabatic condition is given at the left side and bottom boundaries. At the top boundary (surface of the model region), 0°C is given. At the right side boundary, the thermal profile depending on the age of subducted slab is given following Stein and Stein (1992).

Additional file

> **Additional file 1: Table S1.** Velocity structure used for locating events. **Table S2.** List of parameters used in the thermal modeling.

Author details
[1]Department of Earth and Planetary Science, The University of Tokyo, 7-3-1, Hongo, Bunkyo, Tokyo 113-0033, Japan. [2]Research Center for Urban Safety and Security, Kobe University, 1-1, Rokkodai, Nada, Kobe, Hyogo 657-8501, Japan.

References
Allis RG, Funnell R, Zhan X (1998) From basins to mountains and back again: NZ basin evolution since 10 Ma. In: Proceedings 9th International Symposium on Water-Rock Interaction. AA Balkema, Rotterdam, Taupo New Zealand, pp 3–7

Andrews DJ (1972) Numerical simulation of sea-floor spreading. J Geophys Res 77(32):6470–6481, doi:10.1029/JB077i032p06470

Ansell JH, Bannister SC (1996) Shallow morphology of the subducted Pacific plate along the Hikurangi margin, New Zealand. Phys Earth Planet In 93(1):3–20, doi:10.1016/0031-9201(95)03085-9

Ballance PF (1976) Evolution of the Upper Cenozoic magmatic arc and plate boundary in northern New Zealand. Earth Planet Sci Lett 28:356–370, doi:10.1016/0012-821X(76)90197-7

Bannister S, Reyners M, Stuart G, Savage M (2007) Imaging the Hikurangi subduction zone, New Zealand, using teleseismic receiver functions: crustal fluids above the forearc mantle wedge. Geophys J Int 169:602–616, doi:10.1111/j.1365-246X.2007.03345.x

Bartlow NM, Wallace LM, Beavan RJ, Bannister S, Segall P (2014) Time-dependent modeling of slow slip events and associated seismicity and tremor at the Hiku- rangi subduction zone, New Zealand. J Geophys Res Solid Earth 119, doi:10.1002/2013JB010609

Brown JR, Beroza GC, Ide S, Ohta K, Shelly DR, Schwartz SY, Rabbel W, Thorwart M, Kao H (2009) Deep low-frequency earthquakes in tremor localize to the plate interface in multiple subduction zones. Geophys Res Lett 36:L19306, doi:10.1029/2009GL040027

Brudzinski MR, Hinojosa Prieto HR, Schlanser KM, Cabral Cano E, Arciniega Ceballos A, Diaz Molina O, DeMets C (2010) Nonvolcanic tremor along the Oaxaca segment of the Middle America subduction zone. J Geophys Res 115:B00A23, doi:10.1029/2008JB006061

Brune JN (1970) Tectonic stress and the spectra of seismic shear waves from earthquakes. J Geophys Res 75(26):4997–5009, doi:10.1029/JB075i026p04997

Burkett ER, Billen MI (2010) Three-dimensionality of slab detachment due to ridge-trench collision: laterally simultaneous buodinage versus tear propagation. G-Cubed 11:Q11012, doi:10.1029/2010GC003286

Byerlee JD (1978) Friction of rocks. Pure Appl Geophys 116:615–626, doi:10.1007/BF00876528

Caristan Y (1982) The transition from high-temperature creep to fracture in Maryland diabase. J Geophys Res 87:6781–6790, doi:10.1029/JB087iB08p06781

Clift P, Vannucchi P (2004) Controls on tectonic accretion versus erosion in subduction zones: implications for the origin and recycling of the continental crust. Rev Geophys 42:RG2001, doi:10.1029/2003RG000127

Delahaye EJ, Townend J, Reyners ME, Rodgers G (2009) Microseismicity but no tremor accompanying slow slip in the Hikurangi subduction zone, New Zealand. Earth Planet Sci Lett 277:21–28, doi:10.1016/j.epsl.2008.09.038

Dziewonski AM, Chou TA, Woodhouse JH (1981) Determination of earthquake source parameters from waveform data for studies of global and regional seismicity. J Geophys Res 86:2825–2852, doi:10.1029/JB086iB04p02825

Ekström G, Nettles M, Dziewonski AM (2012) The global CMT project 2004–2010: centroid-moment tensors for 13,017 earthquakes. Phys Earth Planet Inter 200–201:1–9, doi:10.1016/j.pepi.2012.04.002

Fagereng Å, Ellis S (2009) On factors controlling the depth of interseismic coupling on the Hikurangi subduction interface, New Zealand. Earth Planet Sci Lett 278:120–130, doi:10.1016/j.epsl.2008.11.033

Fry B, Chao K, Bannister S, Peng Z, Wallace L (2011) Deep tremor in New Zealand triggered by the 2010 Mw8.8 Chile earthquake. Geophys Res Lett 38:L15306, doi:10.1029/2011GL048319

Furukawa Y (1995) Temperature structure in the crust of the Japan arc and the thermal effect of subduction. In: Terrestrial heat flow and geothermal energy in Asia. AA Balkema, Rotterdam, pp 203–219

Gomberg J, the Cascadia 2007 and Beyond Working Group (2010) Slowslip phenomena in Cascadia from 2007 and beyond: a review. Bull Geol Soc Am 122:963–978, doi:10.1130/B30287.1

Ide S (2010) Striations, duration, migration and tidal response in deep tremor. Nature 466:356–359, doi:10.1038/nature09251

Ide S (2012) Variety and spatial heterogeneity of tectonic tremor worldwide. J Geophys Res 117:B03302, doi:10.1029/2011JB008840

Ide S, Shelly DR, Beroza GC (2007) Mechanism of deep low frequency earthquakes: further evidence that deep non-volcanic tremor is generated by shear slip on the plate interface. Geophys Res Lett 34:L03308, doi:10.1029/2006GL028890

Ito Y, Hino R, Kido M, Fujimoto H, Osada Y, Inazu D, Ohta Y, Iinuma T, Ohzono M, Miura S, Mishina M, Suzuki K, Tsuji T, Ashi J (2013) Episodic slow slip events

in the Japan subduction zone before the 2011 Tohoku-Oki earthquake. Tectonophysics 600:14–26, doi:10.1016/j.tecto.2012.08.022

Kamp PJJ (1999) Tracking crustal processes by FT thermochronology in a forearc high (Hikurangi margin, New Zealand) involving Cretaceous subduction termination and mid-Cenozoic subduction initiation. Tectonophysics 307:313–343, doi:10.1016/S0040-1951(99)00102-X

Kato A, Obara K, Igarashi T, Tsuruoka H, Nakagawa S, Hirata N (2012) Propagation of slow slip leading up to the 2011 Mw 9.0 Tohoku-Oki earthquake. Science 335(6069):705–708, doi:10.1126/science.1215141

Kim MJ, Schwartz SY, Bannister S (2011) Non-volcanic tremor associated with the March 2010 Gisborne slow slip event at the Hikurangi subduction margin, New Zealand. Geophys Res Lett 38:L14301, doi:10.1029/2011GL048400

Lewis KB, Collot JY, Lallemande SE (1998) The dammed Hikurangi Trough: a channel-fed trench blocked by subducting seamounts and their wake avalanches (New Zealand–France GeodyNZ Project). Basin Res 10(4):441–468, doi:10.1046/j.1365-2117.1998.00080.x

Liu Z, Owen S, Dong D, Lundgren P, Webb F, Hetland E, Simons M (2010) Estimation of interplate coupling in the Nankai trough, Japan using GPS data from 1996 to 2006. Geophys J Int 181:1313–1328, doi:10.1111/j.1365-246X.2010.04600.x

McCaffrey R, Wallace LM, Beavan J (2008) Slow slip and frictional transition at low temperature at the Hikurangi subduction zone. Nat Geosci 1:316–320, doi:10.1038/ ngeo178

Molnar P, England P (1995) Temperatures in zones of steady-state underthrusting of young oceanic lithosphere. Earth Planet Sci Lett 131:57–70, doi:10.1016/ 0012-821X(94)00253-U

Nicol A, Wallace LM (2007) Temporal stability of deformation rates: comparison of geological and geodetic observations, Hikurangi subduction margin, New Zealand. Earth Planet Sci Lett 258:397–413, doi:10.1016/ j.epsl.2007.03.039

Obara K (2002) Nonvolcanic deep tremor associated with subduction in southwest Japan. Science 296:1679–1681, doi:10.1126/science.1070378

Payero JS, Kostoglodov V, Shapiro N, Mikumo T, Iglesias A, Pe'rez-Campos X, Clayton RW (2008) Nonvolcanic tremor observed in the Mexican subduction zone. Geophys Res Lett 35:L07305, doi:10.1029/2007GL032877

Peacock SM (2009) Thermal and metamorphic environment of subduction zone episodic tremor and slip. J Geophys Res 114:B00A07, doi:10.1029/2008JB005978

Peterson CL, Christensen DH (2009) Possible relationship between nonvolcanic tremor and the 1998–2001 slow slip event, south central Alaska. J Geophys Res 114:B06302, doi:10.1029/2008JB006096

Pollack HN, Hurter SJ, Johnson JR (1993) Heat flow from the Earth's interior: analysis of the global data set. Rev Geophys 31:267–280, doi:10.1029/ 93RG01249

Rait G, Chanier F, Waters D (1991) Landward and seaward-directed thrusting accompanying the onset of subduction beneath New Zealand. Geology 19:230–233, doi:10.1130/0091-7613

Reyners M, Eberhart–Phillips D, Stuart G, Nishimura Y (2006) Imaging subduction from the trench to 300 km depth beneath the central North island, New Zealand, with Vp and Vp/Vs. Geophys J Int 165:565–583, doi:10.1111/j.1365-246X.2006.02897.x

Rogers G, Dragert H (2003) Episodic tremor and slip on the Cascadia subduction zone: the chatter of silent slip. Science 300:1942–1943, doi:10.1126/ science.1084783

Rubinstein JL, Vidale JE, Gomberg J, Bodin P, Creager KC, Malone SD (2007) Non-volcanic tremor driven by large transient shear stresses. Nature 448:579–582, doi:10.1038/nature06017

Seno T (2009) Determination of the pore fluid pressure ratio at seismogenic megathrusts in subduction zones: implications for strength of asperities and Andean-type mountain building. J Geophys Res 114:B05405, doi:10.1029/ 2008JB005889

Shelly DR, Beroza GC, Ide S, Nakamula S (2006) Low-frequency earthquakes in Shikoku, Japan, and their relationship to episodic tremor and slip. Nature 442:188–191, doi:10.1038/nature04931

Shelly DR, Beroza GC, Ide S (2007a) Non-volcanic tremor and low-frequency earthquake swarms. Nature 446(7133):305–307, doi:10.1038/nature05666

Shelly DR, Beroza GC, Ide S (2007b) Complex evolution of transient slip derived from precise tremor locations in western Shikoku, Japan. G-Cubed 8:Q10014, doi:10.1029/2007GC001640

Shibazaki B, Obara K, Matsuzawa T, Hirose H (2012) Modeling of slow slip events along the deep subduction zone in the Kii Peninsula and Tokai regions, southwest Japan. J Geophys Res 117:B06311, doi:10.1029/2011JB009083

Shimamoto T (1986) Transition between frictional slip and ductile flow for halite shear zones at room temperature. Science 231:711–714, doi:10.1126/ science.231.4739.711

Shimamoto T (1989) Mechanical behaviours of simulated halite shear zones: Implications for the seismicity along subducting plate-boundaries. In: Karato S, Toriumi M (eds) Rheology of Solids and of the Earth. Oxford Univ. Press, Oxford, U. K, pp 351–373

Stein CA, Stein S (1992) A model for the global variation in oceanic depth and heat flow with lithospheric age. Nature 359:123–129, doi:10.1038/359123a0

Taylor B (2006) The single largest oceanic plateau: Ontong Java–Manihiki–Hikurangi. Earth Planet Sci Lett 241:372–380, doi:10.1016/j.epsl.2005.11.049

Torii Y, Yoshioka S (2007) Physical conditions producing slab stagnation: constraints of the Clapeyron slope, mantle viscosity, trench retreat, and dip angles. Tectonophysics 445:200–209, doi:10.1016/j.tecto.2007.08.003

Townend J (1997) Estimates of conductive heat flow through bottom-simulating reflectors on the Hikurangi and southwest Fiordland continental margins, New Zealand. Mar Geol 141:209–220, doi:10.1016/S0025-3227(97)00073-X

van Keken PE, Hacker BR, Syracuse EM, Abers GA (2011) Subduction factory: 4. Depth-dependent flux of H2O from subducting slabs worldwide. J Geophys Res 116:B01401

Wada I, Wang K (2009) Common depth of slab-mantle decoupling: reconciling diversity and uniformity of subduction zones. G-Cubed 10:Q10009, doi:10.1029/2009GC002570

Wallace LM, Beavan J (2010) Diverse slow slip behavior at the Hikurangi subduction margin, New Zealand. J Geophys Res 115:B12402, doi:10.1029/ 2010JB007717

Wallace LM, Eberhart-Phillips D (2013) Newly observed, deep slow slip events at the central Hikurangi margin, New Zealand: implications for downdip variability of slow slip and tremor, and relationship to seismic structure. Geophys Res Lett 40:5393–5398, doi:10.1002/2013GL057682

Wallace LM, Beavan J, McCaffrey R, Darby D (2004) Subduction zone coupling and tectonic block rotations in the North Island, New Zealand. J Geophys Res 109:B12406, doi:10.1029/2004JB003241

Wallace LM, Reyners M, Cochran U, Bannister S, Berryman K, Downes G, Eberhart–Phillips D, Fagereng A, Ellis S, Nicol A, McCaffrey R, Beavan JR, Hemrys S, Sutherland R, Barker DHN, Litchfield N, Townend J, Robinson R, Bell R, Wilson K, Power W (2009) Characterizing the seismogenic zone of a major plate boundary subduction thrust: Hikurangi Margin, New Zealand. G-Cubed 10:Q10006, doi:10.1029/2009GC002610

Wallace LM, Beavan J, Bannister S, Williams C (2012) Simultaneous long-term and short-term slow slip events at the Hikurangi subduction margin, New Zealand: implications for processes that control slow slip event occurrence, duration, and migration. J Geophys Res 117:B11402, doi:10.1029/2012JB009489

Wessel P, Smith WH (1991) Free software helps map and display data. Eos Trans AGU 72(41):441–446, doi:10.1029/90EO00319

Williams CA, Eberhart-Phillips D, Bannister S, Barker DHN, Henrys S, Reyners M, Sutherland R (2013) Revised interface geometry for the Hikurangi subduction zone. New Zealand Seismol Res Lett 84(6):1066–1073, doi:10.1785/ 0220130035

Yabe S, Ide S (2013) Repeating deep tremors on the plate interface beneath Kyushu, southwest Japan. Earth Planets Space 65(1):17–23, doi:10.5047/ eps.2012.06.001

Yoshioka S, Sanshadokoro H (2002) Numerical simulations of deformation and dynamics of horizontally lying slabs. Geophys J Int 151:69–82, doi:10.1046/ j.1365-246X.2002.01735.x

Yoshioka S, Suminokura Y, Matsumoto T, Nakajima J (2013) Two-dimensional thermal modeling of subduction of the Philippine Sea plate beneath southwest Japan. Tectonophysics 608:1094–1108, doi:10.1016/j.tecto.2013.07.003